

Initial Evaluation of the USNO Rubidium Fountain

S. Peil,* S. Crane, T. Swanson and C. R. Ekstrom
Clock Development Division, U.S. Naval Observatory
Washington, D.C. 20392

*Electronic address: peil@atom.usno.navy.mil

We discuss the first rubidium atomic fountain at the U. S. Naval Observatory, NRF1, which has been built as a prototype for future devices to be included in the USNO timescale. The system has demonstrated a short-term Allan deviation of $1.35 \times 10^{-13}/\tau^{1/2}$ when measured against a hydrogen maser. We have directly compared NRF1's performance to that of our cesium fountain, NCF, demonstrating integration as $1/\tau^{1/2}$ below 1×10^{-15} , and performance that is consistent with 7×10^{-16} at 11 hours.

1. INTRODUCTION

The USNO Master Clock relies on an ensemble of more than 50 commercial cesium-beam clocks and a dozen active hydrogen masers. The timescale utilizes the good short-term performance of the hydrogen masers and is steered in the long term to the cesium clocks. Future improvements to the Master Clock will be based on introducing advanced clock technology for more rapid and robust characterization of maser frequency drift. A program to build six rubidium atomic fountains for this purpose is underway.

II. FOUNTAIN DESIGN

Continuous, long-term operation in a stable environment requires a robust, compact fountain design. The entire system, described in detail elsewhere [1], will be contained in three 'equipment racks', one of which is the physics package. The other two racks contain computer control, electronics, and a miniature rack-mounted optical table [2].

A cut-away of the physics package of NRF1 is shown in Fig. 1(a). The physics package is enclosed in a set of three magnetic shields which provide a low magnetic-field environment for molasses cooling. Thus, all vacuum and optical components are required to be completely nonmagnetic.

Atoms are loaded into either a MOT with a modest magnetic-field gradient (2 G/cm along the axial direction) or a $\sigma^+ - \sigma^-$ optical molasses. All of the characterization presented here uses MOT loading. After launching, cooling and state-selecting, we end up with $\sim 10^7$ atoms at 1.5 μ K. We run the fountain as a frequency reference by interrogating the central, ~ 1 Hz

wide Ramsey fringe via phase modulation of the 6.8 GHz microwave drive.

(a)

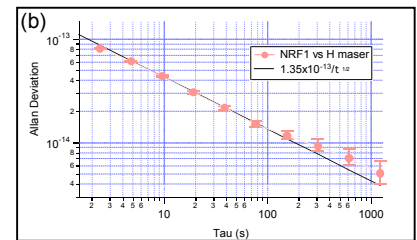


Figure 1 (a) Cross-sectional view of the vacuum chamber and optical couplers of NRF1. All of these components are made from completely nonmagnetic materials. (b) Short-term performance when measured against a hydrogen maser is as good as $1.35 \times 10^{-13}/\tau^{1/2}$. Deviation from white-frequency noise ($1/\tau^{1/2}$ behavior) due to maser frequency fluctuations occurs here at several hundred seconds.

III. CHARACTERIZATION

For typical fountain operation, the microwave interrogation drive is generated from the 5 MHz output of a BVA quartz crystal that is phase-locked to a hydrogen maser with a time constant of ~ 3 seconds. In this configuration, we can see a short-term Allan deviation of $1.35 \times 10^{-13}/\tau^{1/2}$ (Fig. 1(b)). After several hours of integration, the fountain-versus-maser performance becomes limited by maser frequency fluctuations, which usually introduce a deviation from

$1/\tau^{1/2}$ behavior at Allan deviations of several parts in 10^{15} .

In order to obtain a better medium-term characterization of NRF1 than we can achieve with a maser, we measure against our cesium fountain, NCF [3]. The method we used to compare the two devices is illustrated in Fig. 2. We generate the microwave drive for each fountain from the same quartz crystal, which we leave unlocked from any reference maser, removing an unnecessary component. The crystal also serves as the reference oscillator for a pair of adjustable frequency synthesizers. Each synthesizer is adjusted by one of the fountains and outputs the crystal frequency steered to that fountain. This ‘open-loop’ steering is carried out with a time constant of ~ 3.5 seconds and does not change the output of the quartz oscillator itself. The phases of the synthesizer outputs are differenced, and the resultant frequency fluctuations versus integration time can be determined.

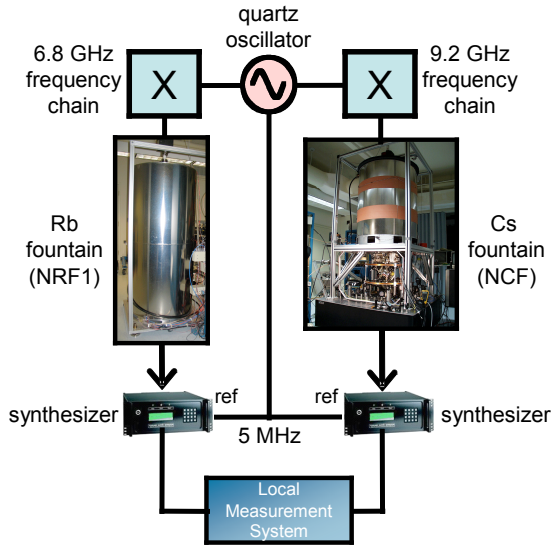


Figure 2 Illustration of the measurement of the relative stability of NRF1 and NCF. For short-term characterization, the crystal can be phase-locked to a maser and either fountain’s performance can be measured. For higher-precision characterization, we unlock the crystal and measure its frequency with each of the two atomic fountains. Comparing these two measurements results in a fountain-to-fountain stability comparison.

This technique was employed for a 3 day run. Each atomic fountain’s measurement of the crystal’s frequency is shown in Fig. 3(a). The noise on the traces indicates a worse short-term performance of NCF compared to NRF1. The plot of Allan deviation versus integration time for this fountain comparison is shown in Fig. 4. The comparison shows a relative stability of $3 \times 10^{-13}/\tau^{1/2}$ and white-frequency noise behavior for integration times up to 11 hours. The relative stability at each point is equal to the quadrature sum of the

individual fountain stabilities at that integration time – additional measurement noise does not contribute at this level of precision.

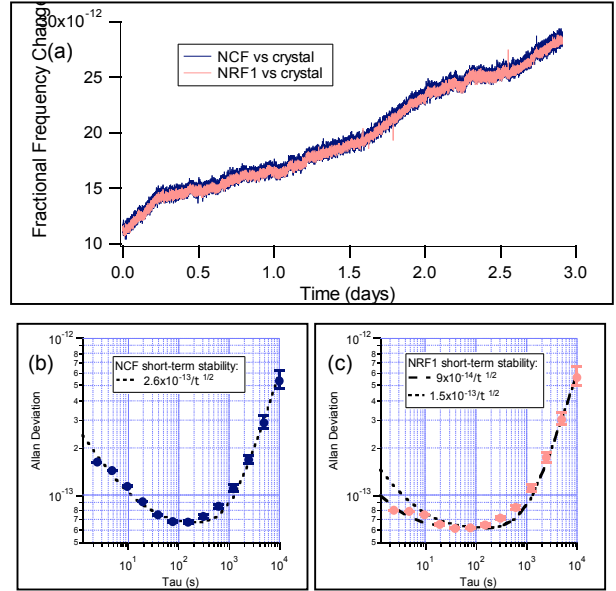


Figure 3 (a) Measurement of the crystal frequency versus time with each fountain. The Allan deviation of this frequency measurement for (b) NCF and (c) NRF1 shows frequency fluctuations from the crystal and from the fountain, enabling a determination of each fountain’s short-term performance.

We can use the crystal frequency measurements of Fig. 3(a) to estimate the performance of each individual fountain – in particular, NRF1. The Allan deviation of each fountain-crystal comparison, shown in Fig. 3(b) & 3(c), exhibits frequency fluctuations comprised of contributions from fountain white-frequency noise ($\tau^{-1/2}$ dependence), crystal frequency flicker (τ^0 dependence), and crystal frequency drift (τ^1 dependence). Plots of the quadrature sum of these three noise types with best-fit coefficients are shown in Fig. 3(b) & 3(c), along with the best value for the white frequency-noise contribution shown in the legend. For NCF, this is $2.6(1) \times 10^{-13}/\tau^{1/2}$, where the error bar represents combined systematic and statistical uncertainties. This is consistent with independent stability measurements made with a hydrogen maser.

Together with the relative fountain stability of $3 \times 10^{-13}/\tau^{1/2}$, this shows that the fountain comparison is limited by the short-term performance of NCF. Consequently, we expect the dependence on τ observed for the relative stability to be representative of the τ -dependence of NCF. We can then infer the stability of NCF for all $\tau \leq 11$ hours from $\sigma_{Cs}(\tau) = 2.6(1) \times 10^{-13}/\tau^{1/2}$. Finally, we can use the fact that the measured relative

stability equals the quadrature sum of the individual fountain stabilities to extract the performance of NRF1 at each τ , shown as the circular data points on Fig. 4. The uncertainties shown are from propagating the uncertainties on the slopes of the $1/\tau^{1/2}$ curves for the comparison data and the estimated NCF performance. The estimated performance of NRF1 is consistent with white-frequency noise behavior over $\frac{1}{2}$ day, reaching a stability of 7×10^{-16} .

The estimated NRF1 data fit well to a $1.5 \times 10^{-13}/\tau^{1/2}$ short-term stability. This value is consistent with what we see when measuring against a maser, but a bit high for what we see against a free-running crystal (Fig. 3(c)). This discrepancy is partly from taking the most conservative estimates for arriving at an expected performance for NRF1.

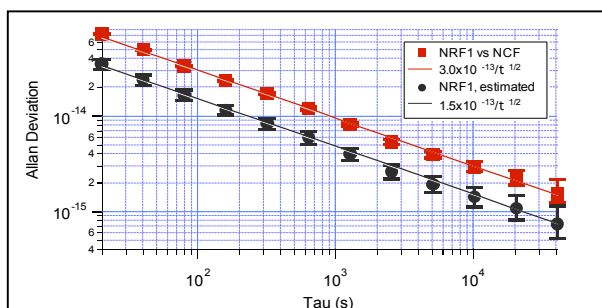


Figure 2 The square data points show the Allan deviation of the relative frequency fluctuations of NRF1 and NCF for integration times up to 11 hours. The circular data points are the estimated Allan deviation of NRF1 from the comparison data and the expected behavior of NCF. The lines are fits to the data.

We would like to be able to measure lower values of the Allan deviation for NRF1, and ultimately reach a noise floor in the fountain comparison. This should be achievable with modest improvements to NCF; by improving the short-term stability, we will compare more efficiently, and by improving the robustness, we will enable comparisons of longer duration.

IV. CONCLUSIONS

We have presented short- and medium-term characterization of NRF1, and have demonstrated a maser-independent method of comparing two atomic fountains. This technique has allowed us to demonstrate white-frequency noise limited performance of NRF1 to an Allan deviation below 1×10^{-15} .

REFERENCES

- [1] S. Peil, S. Crane, T. Swanson, and C. R. Ekstrom, "Design and Preliminary Characterization of the USNO Rubidium Fountain," Proceedings of the IEEE International Frequency Control Symposium, 2005, pp. 304-307.
- [2] S. Crane, S. Peil, and C. R. Ekstrom, "Miniaturized Atomic Fountain Optical Table," Proceedings of the IEEE International Frequency Control Symposium, 2005, pp. 301-303.
- [3] C. R. Ekstrom, E. A. Burt, and T. B. Swanson, "Characterization of the USNO Cesium Fountain," Proceedings of the IEEE Frequency Control Symposium, 2001, pp. 53-56.